

# Rise and fall of laser-intensity effects in spectrally resolved Compton process

U. Hernandez Acosta<sup>1,2,3</sup>, A. I. Titov<sup>4</sup>, B. Kämpfer<sup>1,2</sup>

<sup>1</sup>*Helmholtz-Zentrum Dresden-Rossendorf, 01314 Dresden, Germany*

<sup>2</sup>*Institut für Theoretische Physik, TU Dresden, 01062 Dresden, Germany*

<sup>3</sup>*Center for Advanced Systems Understanding, Untermarkt 20, 02826 Görlitz, Germany and*

<sup>4</sup>*Bogoliubov Laboratory of Theoretical Physics, JINR, Dubna 141980, Russia*

(Dated: May 26, 2021)

The spectrally resolved differential cross section of Compton scattering,  $d\sigma/d\omega'|_{\omega'=const}$ , rises from small towards larger laser intensity parameter  $\xi$ , reaches a maximum, and falls towards the asymptotic strong-field region. Expressed by invariant quantities:  $d\sigma/du|_{u=const}$  rises from small towards larger values of  $\xi$ , reaches a maximum at  $\xi_{max} = \frac{4}{9}\mathcal{K}um^2/k \cdot p$ ,  $\mathcal{K} = \mathcal{O}(1)$ , and falls at  $\xi > \xi_{max}$  like  $\propto \xi^{-3/2} \exp\left(-\frac{2um^2}{3\xi k \cdot p}\right)$  at  $u \geq 1$ . [The quantity  $u$  is the Ritus variable related to the light-front momentum-fraction  $s = (1+u)/u = k \cdot k'/k \cdot p$  of the emitted photon (four-momentum  $k'$ , frequency  $\omega'$ ), and  $k \cdot p/m^2$  quantifies the invariant energy in the entrance channel of electron (four-momentum  $p$ , mass  $m$ ) and laser (four-wave vector  $k$ ).] Such a behavior of a differential observable is to be contrasted with the laser intensity dependence of the total probability,  $\lim_{\chi=\xi k \cdot p/m^2, \xi \rightarrow \infty} \mathbb{P} \propto \alpha\chi^{2/3}m^2/k \cdot p$ , which is governed by the soft spectral part.

We combine the hard-photon yield from Compton with the seeded Breit-Wheeler pair production in a folding model and obtain a rapidly increasing  $e^+e^-$  pair number at  $\xi \lesssim 4$ . Laser bandwidth effects are quantified in the weak-field limit of the related trident pair production.

PACS numbers: 12.20.Ds, 13.40.-f, 23.20.Nx

Keywords: non-linear Compton scattering, nonlinear Breit-Wheeler pair production, strong-field QED

## I. INTRODUCTION

Quantum Electro-Dynamics (QED) as pillar of the standard model (SM) of particle physics possesses a positive  $\beta$  function [1] which makes the running coupling strength  $\alpha(\mathfrak{s})$  increasingly with increasing energy/momentum scale  $\mathfrak{s}$  [2]. In contrast, Quantum Chromo-Dynamics (QCD) as another SM pillar possesses a negative  $\beta$  function due to the non-Abelian gauge group [1], giving rise to the asymptotic freedom,  $\lim_{\mathfrak{s} \rightarrow \infty} \alpha_{QCD}(\mathfrak{s}) \rightarrow 0$ , i.e. QCD has a truly perturbative limit. In contrast,  $\lim_{\mathfrak{s} \rightarrow 0} \alpha(\mathfrak{s}) \rightarrow 1/137.0359895(61)$  is not such a strict limit, nevertheless, QED predictions/calculations of some observables agree with measurements within 13 digits, see [3–5] for some examples. The situation in QED becomes special when considering processes in external (or background) fields: One can resort to the Furry (or bound-state) picture, where the (tree-level) interactions of an elementary charge (e.g. an electron) with the background are accounted for in all orders, and the interactions with the quantized photon field remains perturbatively in powers of  $\alpha$ . However, the Ritus-Narozhny (RN) conjecture [6–10] argues that the effective coupling becomes  $\alpha\chi^{2/3}$ , meaning that the Furry picture expansion beaks down at  $\alpha\chi^{2/3} > 1$  [11–14] (for the definition of  $\chi$  see below) and one enters a genuinely non-perturbative regime. The latter requires adequate calculation procedures, as the lattice regularized approaches, which are standard since many years in QCD, e.g. in evaluations of observables in the soft sector where  $\alpha_{QCD} > 1$ , cf. [15]. (In QED itself, an analog situation is met in the Coulomb field of nuclear systems with proton numbers  $Z > Z_{crit} \approx 173$ : if  $\alpha Z_{crit} > 1$  the

QED vacuum beak-down sets in; cf. [16] for the actual status of that field).

With respect to increasing laser intensities the quest for the possible break-down of the Furry picture expansion in line with the RN conjecture becomes, besides its principal challenge, also of “practical” interest, whether one can explore experimentally this yet uncharted regime of QED. (For other configurations, e.g. beam-beam interactions, cf. [17]). A prerequisite would be to find observables which display the typical dependence  $\propto \alpha\chi^{2/3}$ , where we denote by  $\alpha$  the above quoted fine-structure constant at  $\mathfrak{s} \rightarrow 0$ . In doing so we resort here to the lowest-order QED processes, that is nonlinear Compton and nonlinear Breit-Wheeler. Both processes seem to be investigated theoretically in depth in the past, however, enjoy currently repeated re-considerations w.r.t. refinements [18–23], establishing approximation schemes [24–28] to be implemented in simulation codes [29–31] or to use them as building blocks in complex processes [32], with the starting point at trident [33–35].

Beginning with Compton scattering ( $p$  and  $p'$  are the *in*- and *out*-electron four-momenta,  $k$  the laser four-momentum, and  $k'$  the *out*-photon’s four-momentum, respectively) the relevant (Lorentz and gauge invariant) variables of the entrance channel are [36]

- (i) the classical intensity parameter of the laser:  $\xi = |e|\mathcal{E}/(m\omega)$ , here expressed by quantities in the lab.:  $\mathcal{E}$  - electric laser field strength,  $\omega$  - the central laser frequency;  $-|e|$  and  $m$  stand for the electron charge and

mass, respectively, and  $e^2/4\pi = \alpha$ ,<sup>1</sup>  
- (ii) the available energy squared:  $k \cdot p/m^2 = (\hat{s}/m^2 - 1)/2$  with  $\hat{s}$  as Mandelstam variable,  
- (iii) the quantum nonlinearity parameter:  $\chi = \xi k \cdot p/m^2$ .  
The latter quantity is often considered as the crucial parameter since in some limits it determines solely the probability of certain processes.  $\chi$  plays also a prominent role in the above mentioned discussion of the RN conjecture, where the Furry picture expansion of QED is argued to break down for  $\alpha\chi^{2/3} > 1$ . References [37, 38] point out that the large- $\chi$  limits, facilitated by either large  $\xi$  (the high-intensity limit) or large  $k \cdot p/m^2$  (the high-energy limit), are distinctively different, with implications for approximation schemes in simulation codes.

Figure 1 exhibits a few selected curves  $\chi = \text{const}$  over the  $\xi$  vs.  $k \cdot p/m^2$  landscape to illustrate the current situation w.r.t. facilities where laser beams and electron beams are (or can be) combined. One has to add the options at E-320 at FACET-II/SLAC [39, 40] and electron beams which are laser-accelerated to GeV scales, e.g. [41–43].

Usually,  $\xi = 1$  is said to mark the the onset of strong-field effects, and the corresponding processes at  $\xi > 1$  are termed by the attribute “nonlinear”. In this respect, the parameters provided by LUXE [44, 45] and FACET-II [39, 40] are interesting:  $\chi = \mathcal{O}(1)$  and above and  $\xi > 1$  as well.<sup>2</sup> In the following we consider the LUXE kinematics (see Fig. 1),  $k \cdot p/m^2 \approx \omega E_e(1 - \cos \Theta) = 0.2078$  in head-on collisions ( $\cos \Theta = -1$ ). Our aim is to quantify a simple observable as a function of  $\xi$ . To be specific, we select the invariant differential cross section  $d\sigma/du$ , where  $u$  is the light-cone momentum-transfer of the *in*-electron to the *out*-photon, related to light-front momentum-fraction of the *out*-photon  $s = \frac{u}{1+u} = \frac{k \cdot k'}{k \cdot p}$ . (The mapping  $u \mapsto \omega'$  and  $d\sigma/du \mapsto d\sigma/d\omega'$  is discussed in [46, 47].) To make the meaning of the Ritus variable  $u$  more explicit let us mention the relation  $u = \frac{e^{-\zeta} \nu' (1 - \cos \Theta')}{1 - e^{-\zeta} \nu' (1 - \cos \Theta')}$ , where  $\nu' \equiv \omega'/m$ , and the electron energy  $E_e$  in lab. determines the rapidity  $\zeta$  via  $E_e = m \cosh \zeta$  and  $\Theta'$  denotes the polar lab. angle of the *out*-photon. We call  $d\sigma/du$  a spectrally resolved observable.

Our note is organized as follows. In section II we briefly recall a few approximations of the laser beam. Section III is devoted to an analysis of the invariant differential cross section  $d\sigma/du$  and its dependence on the laser intensity parameter  $\xi$  in nonlinear Compton scattering. That is, we are going up and down on the vertical dashed line with label LUXE in Fig. 1 around the point  $\chi = 1$  or  $\xi = 1$ . The discussion section IV (i) relates the cross section to the probability and (ii) considers a folding model which uses the hard-photon spectrum emerging from Compton

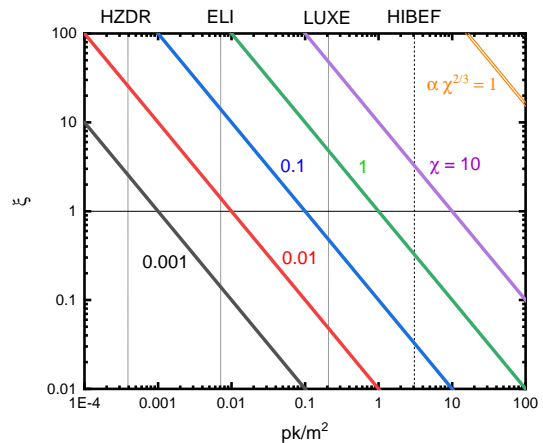


FIG. 1: Curves of  $\chi = \text{const}$  over the  $\xi$  vs.  $k \cdot p/m^2$  plane for  $\chi = 0.001, 0.01, 0.1, 1$  and  $10$ . The double-line depicts the curve  $\alpha\chi^{2/3} = 1$ . Vertical thin lines are for maximum values of  $k \cdot p/m^2$  in reach at various electron accelerators (HZDR [48]:  $E_e = 33$  MeV, ELI [49]:  $E_e = 600$  MeV, LUXE [44, 45]:  $E_e = 17.5$  GeV) in combination with a high-intensity optical laser (we use  $\omega = 1.55$  eV as representative frequency). The vertical dotted line indicates a possible combination of the European XFEL ( $\omega = 10$  keV) with a laser-accelerated electron beam ( $E_e = 10$  MeV) available in the high-energy density cave of the HIBEF collaboration [50]. The horizontal delineation line  $\xi = 1$  is thought to highlight the onset of the strong-field region above.

scattering as seed for subsequent Breit-Wheeler pair production; a brief discussion of (iii) bandwidth effects relevant for sub-threshold trident pair production complements this section. We conclude in section V. The appendix A recalls a few basic elements of the one-photon Compton process.

## II. LASER MODELS

In plane-wave approximation<sup>3</sup> the laser (circular polarization) can be described by the four-potential in axial gauge,  $A = (0, \vec{A})$ , with

$$\vec{A} = f(\phi) (\vec{a}_x \cos \phi + \vec{a}_y \sin \phi) \quad (1)$$

where  $\vec{a}_x^2 = \vec{a}_y^2 = m^2 \xi^2 / e^2$ ; the polarization vectors  $\vec{a}_x$  and  $\vec{a}_y$  are mutually orthogonal. We ignore a possible

<sup>1</sup> We employ natural units with  $\hbar = c = 1$ .

<sup>2</sup> Despite high intensities at XFELs, e.g.  $I \rightarrow 10^{22}$  W/cm<sup>2</sup>, the intensity parameter  $\xi = \frac{7.5 \text{ eV}}{\omega} \sqrt{\frac{I}{10^{20} \text{ W/cm}^2}}$  [36] is small due to the high frequency, e.g.  $\omega = 1 - 25$  keV.

<sup>3</sup> Due to the high symmetry, the exact solutions of the Dirac equation in a plane-wave background are in a comfortably compact form enabling an easy processing in evaluations of matrix elements. Without such a high symmetry, much more attempts are required [51–53]. For some useful parameterizations of laser beams, see [54–56] and further citations therein. The relevance of the Fourier-zero mode of (non-)unipolar planar fields is mentioned in [57].

non-zero value of the carrier envelope phase and focus on symmetric envelope functions  $f(\phi)$  w.r.t. the invariant phase  $\phi = k \cdot x$ . One may classify the such a model class as follows.

- 1) Laser pulses:  $\lim_{\phi \rightarrow \pm\infty} f(\phi) = 0$ ,
- 2) Monochromatic beam:  $f(\phi) = 1$ ,
- 3) Constant cross field (ccf):  $\vec{A} = \phi \vec{a}_x$ .

The probabilities for the constant cross field option 3) coincide with certain limits of the plane-wave model 2) [58]; in [47] they are related to the large- $\xi$  limit. Item 1) could be divided into several further sub-classes, such as 1.1): finite support region of the pulse, i.e.  $f(|\phi| > \phi_{pulse\ length}) = 0$ ,  $\phi_{pulse\ length} < \infty$ , and 1.2): far-extended support region, i.e.  $\lim_{\phi \rightarrow \pm\infty} f(\phi) \rightarrow 0$ , together with non-zero carrier envelope phase, asymmetric pulse shape, frequency chirping, polarization gating etc. A specific class is 1.1) with flat-top section, e.g. a box envelope  $\square$  (cf. [59] for a recent explication) belonging to  $C^0$ , or  $\cos^2 \otimes \square$  belonging to  $C^2$  or the construction in [60] belonging to  $C^\infty$ . Examples for item 1.2) are Gauss, super-Gauss (employed in [61], for instance), symmetrized Fermi function [62, 63],  $1/\cosh$  etc. The monochromatic beam, item 2), corresponds formally to an infinitely long flat-top “pulse”, abbreviated hereafter by IPA as acronym of infinite pulse approximation. It may be considered as special case of 1.1) with  $\phi_{pulse\ length} \rightarrow \infty$ . FPA stands henceforth for the finite pulse-length plane-wave approximation.

To be specific, we employ here 1.2) with  $f(\phi) = 1/\cosh(\phi/\pi N)$ , where  $N$  characterizes the number of oscillations in that pulse interval, where  $f(\phi)$  is significantly larger than zero (see [47, 62, 64] for the formalism), and IPA from 2). The laser model of class 1.1) is employed in subsection IV C.

### III. COMPTON: DIFFERENTIAL INVARIANT CROSS SECTION

Let us consider the above pulse envelope function  $f(\phi) = 1/\cosh(\phi/(\pi N))$  to elucidate the impact of a finite pulse duration and contrast it later on with the monochromatic laser beam model and some approximations thereof. Differential spectra  $d\sigma/du$  as a function of  $u$  are exhibited in Fig. 2 in the region  $u \leq 3$  for several values of  $\xi \leq 1$  for the FPA (dashed curves) and IPA (solid curves) models recalled below. This complements figures 1 – 3 in [47]. One observes that the harmonic structures (which would become more severe for linear polarization, see [47]) fade away at larger values of  $u$  and  $\xi$ . Therefore, we are going to analyze that region in parameter space. There, IPA results represent reasonably well the trends of the more involved FPA calculations.

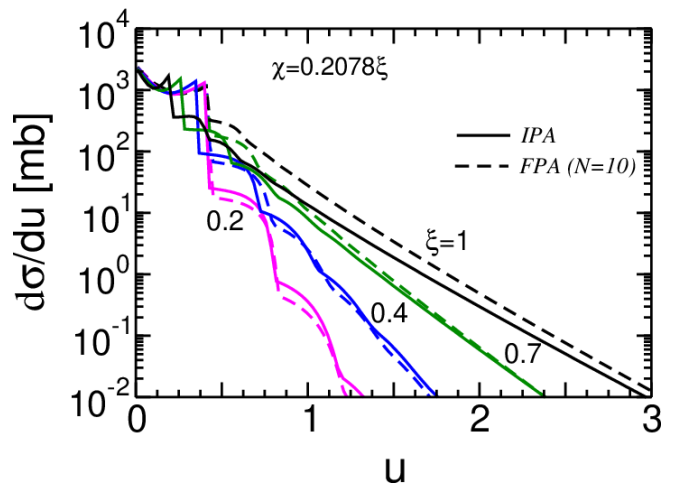


FIG. 2: Invariant differential cross section  $d\sigma(u, \xi, k \cdot p/m^2)/du$  as a function of  $u$  for several values of  $\xi$ ,  $\xi = 0.2$  (magenta),  $0.4$  (blue),  $0.7$  (green) and  $1$  (black). The dashed curves (label FPA) are for pulses according to Eq. (1) with  $f(\phi) = 1/\cosh(\phi/(\pi N))$  for  $N = 10$ . The IPA results for a monochromatic laser beam are depicted by solid curves (with the limit  $d\sigma_{IPA}/du|_{u \rightarrow 0} = 2\pi\alpha^2/k \cdot p$  independent of  $\xi$ ). The pronounced harmonic structures around the Klein-Nishina (KN) edge  $u_{KN} \approx 0.416$  are irrelevant for the subsequent discussion and, therefore, do not need a detailed representation. For  $\chi = \xi k \cdot p/m^2 = 0.2078\xi$ .

#### A. Numerical results

In particular, we consider now  $d\sigma(u, \xi, k \cdot p/m^2)/du$  as a function of  $\xi$  for several constant values of  $u$ ,  $u = 0.5, 1, 2, 4$  and  $8$ , for  $k \cdot p/m^2 = 0.2078$  – a value which is motivated by the LUXE opportunities [44, 45]. The solid, dotted and dashed curves in Fig. 3 are based on easily accessible models [58]:

- monochromatic model (IPA) (cf. equations (15, 16) in [47]):

$$\frac{d\sigma_{IPA}}{du} = \frac{2\pi\alpha^2}{k \cdot p} \frac{1}{(1+u)^2} \sum_{n=1}^{\infty} \Theta(u_n - u) F_n(z_n), \quad (2)$$

$$F_n = -\frac{2}{\xi^2} J_n^2(z_n) + A (J_{n+1}^2(z_n) + J_{n-1}^2(z_n) - 2J_n^2(z_n)) \quad (3)$$

with  $A = 1 + \frac{u^2}{2(1+u)}$ ,  $z_n(u, u_n) = \frac{2n\xi}{\sqrt{1+\xi^2}} \sqrt{\frac{u}{u_n} (1 - \frac{u}{u_n})}$ , and  $u_n = \frac{2nk \cdot p}{m^2(1+\xi^2)}$  ( $J_n$ 's denote Bessel functions of first kind);

- IPA–large- $\xi$  approximation (cf. equation (21) in [47]):

$$\frac{d\sigma_{large-\xi}}{du} = -\frac{4\pi\alpha^2}{m^2\xi} \frac{1}{\chi} \frac{1}{(1+u)^2} \mathcal{F}_C \quad (4)$$

$$\mathcal{F}_C = \int_z^{\infty} dy \Phi(y) + \frac{2}{z} \left[ 1 + \frac{u^2}{2(1+u)} \right] \Phi'(z) \quad (5)$$

where  $\Phi(z)$  and  $\Phi'(z)$  stand for the Airy function and its derivative with arguments  $z = (u/\chi)^{2/3}$  where  $\chi =$

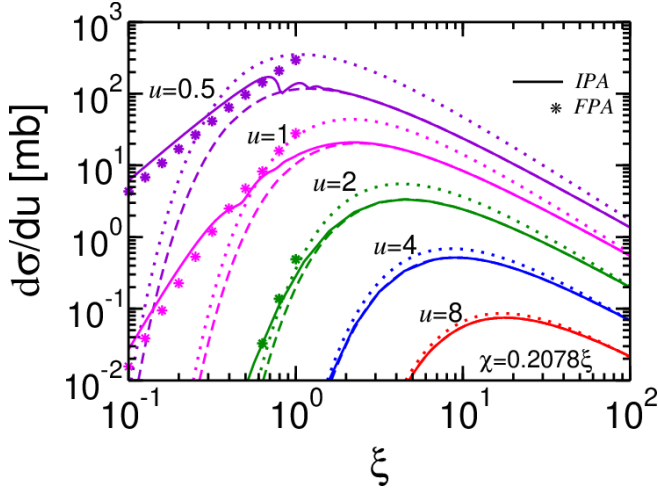


FIG. 3: Invariant differential cross section  $d\sigma(u = \text{const}, \xi, k \cdot p/m^2)/du$  as a function of  $\xi$  for several values of  $u$ ,  $u = 0.5, 1, 2, 4$  and  $8$ ; for  $k \cdot p/m^2 = 0.2078$ . The asterisks depict results of short laser pulses with envelope function  $f(\phi) = 1/\cosh(\phi/(\pi N))$  for  $N = 10$ ,  $d\sigma_{FPA}/du$ , Eq. (7). The solid curves are for the monochromatic laser beam model  $d\sigma_{IPA}/du$ , Eq. (2), while dashed (dotted) curves are based on  $d\sigma_{large-\xi}/du$ , Eq. (4) ( $d\sigma_{large-\xi, large-u}/du$ , Eq. (6)).

$\xi k \cdot p/m^2$ ;

• large- $\xi$ -large- $u$  approximation (cf. equation (22) in [47]):

$$\frac{d\sigma_{large-\xi, large-u}}{du} = \frac{2\sqrt{\pi}\alpha^2}{m^2\xi} \chi^{-1/2} u^{-3/2} \exp\left(-\frac{2u}{3\chi}\right). \quad (6)$$

The asterisks in Fig. 3 depict results of the pulse model (FPA) described in [47, 62] (cf. equations (5 - 14) in [47]):

$$\frac{d\sigma_{FPA}}{du} = \frac{\alpha^2}{k \cdot p} \frac{1}{(1+u)^2} \int_0^\infty d\ell \Theta\left(\frac{um^2}{2k \cdot p} - \ell\right) w(\ell), \quad (7)$$

$$w(\ell, z) = \int_0^{2\pi} d\phi_{e'} \left[ -\frac{2}{\xi^2} |\tilde{Y}_\ell(z_\ell)|^2 \right] \quad (8)$$

$$+ A \left( |Y_{\ell-1}(z_\ell)|^2 + |Y_{\ell+1}(z_\ell)|^2 - 2\text{Re}\tilde{Y}_\ell(z_\ell)X_\ell^*(z_\ell) \right)$$

with  $A$  as above,  $z_\ell(u, \ell) = 2\ell\xi\sqrt{\frac{u}{u_\ell}(1-\frac{u}{u_\ell})}$  and  $u_\ell = \frac{2\ell k \cdot p}{m^2}$ . The basic functions  $Y_\ell, \tilde{Y}_\ell, X_\ell$  and their  $\phi_{e'}$  dependence are spelled out in [47, 62]; they depend crucially on the pulse envelope function  $f(\phi)$ . (Due to numerical accuracy reasons in integrating highly oscillating functions, these evaluations are constrained presently to not too large values of  $\xi$ .) The common basis of these models is sketched in Appendix A.

We consider in Fig. 3 only  $u > u_{KN} = 2k \cdot p/m^2$ , since at the Klein-Nishina (KN) edge the harmonic structures become severe, as seen in Fig. 2. The striking feature seen in Fig. 3 is the pronounced  $\cap$  shape, which we coin “rise and fall” of laser intensity effects. At small  $\xi$ , the realistic FPA ( $N = 10$ ) results (asterisks) and the IPA model (solid curves) follow the same trends, consistent with Fig. 2. The large- $\xi$  and large- $\xi$ -large- $u$  approximations (dashed and dotted curves) are not supposed to apply in that region. However, they become useful representatives at large  $\xi$ .

## B. The rise

Some guidance of the rising parts of the FPA results in Fig. 3 can be gained by the monochromatic model. Casting Eq. (3) in the form

$$F_n = -\frac{2(1-\Xi^2)}{\Xi^2} J_n^2(\Xi x_n) + A (J_{n+1}^2(\Xi x_n) + J_{n-1}^2(\Xi x_n) - 2J_n^2(\Xi x_n)) \quad (9)$$

with  $\Xi^2 = \xi^2/(1+\xi^2)$  and  $x_n(u) = 2n\sqrt{\frac{u}{u_n}(1-\frac{u}{u_n})}$  and expanding in powers of  $\Xi$  yields for the first terms

$$F_1 = \frac{1}{2}(2A - x_1^2) - \frac{x_1^2}{8}(8A - x_1^2 - 4)\Xi^2 + \frac{x_1^4}{384}(90A - 5x_1^2 - 48)\Xi^4 + \mathcal{O}(\Xi^6), \quad (10)$$

$$F_2 = \frac{x_2^2}{32}(8A - x_2^2)\Xi^2 - \frac{x_2^4}{192}(18A - x_2^2 - 6)\Xi^4 + \mathcal{O}(\Xi^6), \quad (11)$$

$$F_3 = \frac{x_3^4}{1152}(18A - x_3^2)\Xi^4 + \mathcal{O}(\Xi^6). \quad (12)$$

Due to the Heavyside  $\Theta$  function in Eq. (2), the leading-order power in  $\Xi$  depends on the value of  $u$ , e.g. for  $u < u_1$ , the series starts with  $\mathcal{O}(\Xi^0)$  and the coefficients of higher orders accordingly sum up. Higher values of  $u$

facilitate higher orders of the leading terms, i.e. the rise becomes steeper since the respective leading-order term is  $\propto \Xi^{2\lfloor u/u_1 \rfloor}$ . This statement is based on the structures in Eqs. (10 - 12), suggesting  $F_n = \sum_{i=n-1} F_n^{(2i)} \Xi^{2i}$  for

the first terms  $F_n^{(2i)}$ , and  $\sum_{n=1}^{\infty} \Theta(u_n - u) F_n = \sum_{n_{min}}^{\infty} F_n$  with  $n_{min} = 1 + \lfloor u/u_1 \rfloor$ . ( $\lfloor \cdot \rfloor$  is the floor operation.)

The series expansion of (9) in powers of  $\Xi$  ignores the sub-leading  $\Xi$  dependence in  $x_n$  via  $u_n = 2n \frac{k \cdot p}{m^2} (1 - \Xi^2)$  but is suitable for  $k \cdot p = const$ .

Analogously considerations apply to the pulse model, cf. section III.C in [62]. An essential role is played by the Fourier transform of the pulse envelope in the limit  $\xi \ll 1$ . It bridges to the IPA for long pulses.

### C. The fall

The maximum of the curves exhibited in Fig. 3 at  $u = \mathcal{O}(1)$  is attained at  $\xi = \mathcal{O}(1)$ , but moves towards larger values of  $\xi$  with increasing values of  $u$ . Remarkably, the often discredited large- $\xi$  and large- $\xi$ -large- $u$  approximations (dotted and dashed curves) deliver results in fair agreement with the IPA results (solid curves) for  $u > 1$ . That is, when being interested in the high-energy photon tails, the simple large- $\xi$ -large- $u$  formula Eq. (6) [58] represents a fairly accurate description supposed  $\xi$  is sufficiently large. Obviously, at  $\xi < 1$  and  $u < 2$ , such an approximation fails quantitatively. (In particular, at  $u < 1$  the harmonic structures in IPA become severe.) Nevertheless, some estimate of the maximum position is provided by  $\xi_{max} \approx \frac{4}{9} u m^2 / k \cdot p$  yielding  $d\sigma/du(\xi_{max}) \approx \frac{2\sqrt{\pi}\alpha^2}{m^2} \frac{k \cdot p}{m^2} \left(\frac{3}{2}\right)^3 e^{-3/2} u^{-3}$ . The asymptotic fall is governed by  $\frac{d\sigma}{du} \propto \frac{1}{m^2} \frac{m^2}{k \cdot p} \xi^{-3/2} u^{-3/2} \exp\left(-\frac{2um^2}{3\xi k \cdot p}\right)$  from Eq. (6).

We emphasize the same pattern of rise and fall of  $d\sigma/d\omega'|_{\omega'=const}$ , see Fig. 4, again for sufficiently large values of  $\omega'$ . The spectrally resolved differential cross section  $d\sigma/d\omega'|_{\omega'=const}$  is directly accessible in experiments. In the strong-field asymptotic region it displays a funneling behavior, i.e. the curves are squeezed into a narrow corridor already in the non-asymptotic  $\xi$  region, in contrast to  $d\sigma/du|_{u=const}$  in Fig. 3.

## IV. DISCUSSION

### A. Cross section vs. probability

The cross section  $\sigma$  and Ritus probability rate  $W$  are related as  $W = \frac{m^4}{4\pi\alpha} \frac{\xi\chi}{q_0} \sigma$  with  $q_0$  denoting the energy component of the quasi-momentum of the *in*-electron. This relation holds true for circular polarization and applies to respective differential quantities too. The different normalization modifies in particular the  $\xi$  dependence: The above emphasized “rise and fall” of  $d\sigma/du$  corresponds to a monotonously rising probability  $dW/du$  as a function of  $\xi$ . Having in mind Ritus’ remark “the cross-sectional concept becomes meaningless” since, at  $\xi \rightarrow \infty$  we have  $\sigma \rightarrow 0$  while  $W$  remains finite [58], we turn in this sub-section to the probability. In doing so we remind the reader of the subtle Ritus notation

$W(\chi) = \frac{1}{\pi} \int_0^\pi d\psi P(\chi \sin \psi)$  in distinguishing the probabilities  $W$  and  $P$ .

We also stress the varying behavior of total (cf. appendix A in [65]) and differential probabilities. Equation (6) emerges as a certain limit of the constant cross field probability [58]  $\frac{dP(\chi, u)}{du} = -V(1+u)^{-2} \mathcal{F}_C(z(\chi, u), u)$  where the prefactor reads  $V = \alpha m^2 / \pi q_0$  and  $\mathcal{F}_C$  is defined in Eq. (5). With respect to the argument  $z = (u/\chi)^{2/3}$  of the Airy functions in Eq. (5), the  $\chi - u$  plane can be divided into the regions I (where  $u > \chi$ ) and II (where  $u < \chi$ ). Furthermore, the combination  $1 + u$  suggests a splitting into  $u < 1$  and  $u > 1$  sub-domains. Picking up the leading-order terms in the related series expansions one arrives at

$$\frac{dP}{du}|_{u \gg \chi} = \frac{V}{2\sqrt{\pi}} \chi^{1/2} \exp\left(-\frac{2u}{3\chi}\right) \times \begin{cases} u^{-1/2} & \text{for } u \ll 1, & (I^<) \\ u^{-3/2} & \text{for } u \gg 1, & (I^>) \end{cases} \quad (13)$$

$$\frac{dP}{du}|_{u \ll \chi} = -V\Phi'(0)\chi^{2/3} \times \begin{cases} 2u^{-2/3} & \text{for } u \ll 1, & (II^<) \\ u^{-5/3} & \text{for } u \gg 1. & (II^>) \end{cases} \quad (14)$$

It is the soft  $u$ -part  $II^<$  of the differential probability in Eq. (14) which essentially determines the total

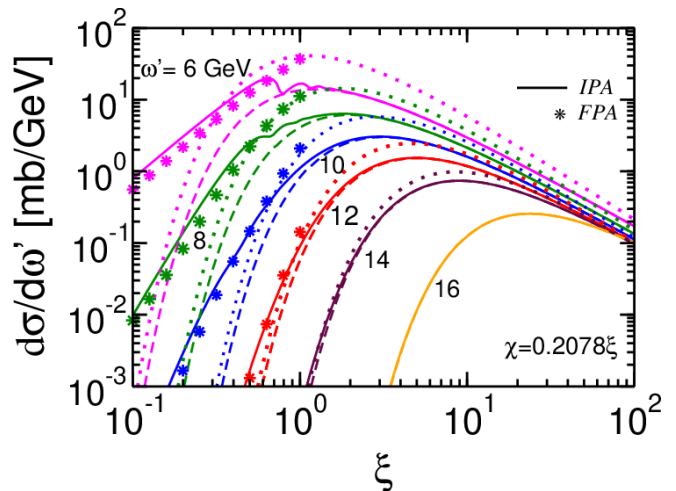


FIG. 4: The same as in Fig. 3 but for  $d\sigma/d\omega'$  as a function of laser intensity parameter  $\xi$  for several constant values of  $\omega'$ .

probability upon  $u$ -integration,<sup>4</sup> i.e. the celebrated result  $P \propto \alpha\chi^{2/3}$  in Ritus notation [58] (stated as  $\lim_{\chi, \xi \rightarrow \infty} \mathbb{P} \propto \alpha\chi^{2/3}m^2/k \cdot p$  in [37]), while the hard  $u$ -part  $I^>$  in Eq. (13) is at the origin of Eq. (6) when converting to cross section. In other words, one has to distinguish the  $\xi$  (or  $\chi$ ) dependence either of integrated or differential observables. In relation to the LUXE plans [44] we mention the photon detector developments [66] which should enable in fact the access to the differential spectra.

## B. Secondary processes: Breit-Wheeler

Instead transferring these considerations to the Breit-Wheeler (BW) process *per se* (cf. [67–74] and further citations below), we estimate now the BW pair production seeded by the hard photons from the above Compton (C) process. The following folding model C $\otimes$ BW is a pure two-step ansatz on the probabilistic level which mimics in a simple manner some part of the trident process<sup>5</sup>  $e_L^- \rightarrow e_L'^- + e_L''^- + e_L^+$  by ignoring (i) the possible off-shell effects and non-transverse components of the intermediate photon (that would be the one-step contribution) and (ii) the anti-symmetrization of the two electrons in the final state (that would be the exchange contribution). Such an ansatz is similar to the one in [75], where however bremsstrahlung $\otimes$ BW has been analyzed. An analog approach has been elaborated in [76] for di-muon production.

Specifically, we consider the two-step cascade process where a GeV-Compton photon with energy  $\omega'$  is produced in the first step, and, in the next step, that GeV-photon interacts with the same laser field producing a BW- $e^+e^-$  pair. We estimate the number of pairs produced in one pulse by

$$N^{e^+e^-} = \int_0^\infty d\omega' \int_0^{T_C} dt \frac{d\Gamma_C(\omega', t)}{d\omega'} \int_t^{T_{BW}} dt' \Gamma_{BW}(\omega', t'), \quad (15)$$

where  $d\Gamma_C(\omega', t)/d\omega'$  is the rate of photons per frequency interval  $d\omega'$  (which corresponds to  $dP/du$  in IV A) emerging from Compton at time  $t \in [0, T_C]$ , and  $\Gamma_{BW}(\omega', t')$  is the rate of Breit-Wheeler pairs generated by a probe photon of frequency  $\omega'$  at lab. frame time-distance  $t' \in$

$[t, T_{BW}]$ . The underlying picture is that of an electron traversing a laser pulse in head-on geometry near to light cone. The passage time of an undisturbed electron would be  $NT_0/2$ ,  $T_0 = 2\pi/\omega$ . Neglecting spatio-temporal variations within the pulse, the final formula becomes  $N^{e^+e^-} = F_t \int_0^{E_e} d\omega' N_0^e \frac{d\Gamma_C(\omega')}{d\omega'} \Gamma_{BW}(\omega')$  upon the restriction  $\omega' < E_e$  and  $F_t = T_C(T_{BW} - T_C/2)$ . A crucial issue is the choice of the formation time(s) [80, 81]. When gluing C $\otimes$ BW on the amplitude level, such a time appears linearly in the pair rate [82]<sup>6</sup> or quadratically in the net probability via overlap light-cone times (cf. [77, 78] for instance). The time-ordered double integral over the C and BW probabilities, yielding the cascade approximation (cf. equation (43) in [78]), is analog to our above formula by folding two rates, which facilitates  $F_t \propto T_0^2$ , if  $T_{C, BW} \propto T_0$ . We attach to the Compton rate the number  $N_0^e = 6 \times 10^9$  of primary electrons per bunch.

In the numerical evaluation we employ the following convenient approximations:

$$\frac{d\Gamma_C}{d\omega'} = -\frac{\alpha m^2}{\pi E_e^2} \mathcal{F}_C(z, u), \quad (16)$$

$$\Gamma_{BW}(\omega') = \frac{\alpha m^2}{\omega'} \mathcal{F}_{BW}, \quad (17)$$

$$\mathcal{F}_{BW} = \sqrt{\frac{3^3}{2^9}} \kappa \exp \left[ -\frac{8}{3\kappa} \left( 1 - \frac{1}{15\xi^2} \right) \right], \quad (18)$$

where  $u = \kappa/(\chi - \kappa)$ ,  $\chi = (k \cdot p)\xi/m^2$ ,  $\kappa = (k \cdot k')\xi/m^2$ , and  $\mathcal{F}_C(z, u)$  with  $z = (u/\chi)^{2/3}$  is defined in Eq. (5). Note the rise of  $\Gamma_{BW}$  and the fall of  $d\Gamma_C/d\omega'$  as a function of  $\omega'$  at fixed values of  $\xi$  and  $k \cdot p$  and laser frequency  $\omega$ , see Fig. 5. Increasing values of  $\xi$  lift  $d\Gamma_C/d\omega'$  somewhat and make it flatter in the intermediate- $\omega'$  region, thus sharpening the drop at  $\omega' \rightarrow E_e$ . Remarkable is the strong impact of increasing  $\xi$  on the BW rate.

One may replace Eq. (5) in (16) by the sum over harmonics expressed by Bessel functions [58] to get an improvement of accuracy in the small- $\omega'$  region:<sup>7</sup>

$$\frac{d\Gamma_C^{IPA}}{d\omega'} = \frac{d\sigma_C^{IPA}}{d\omega'} \frac{\xi^2 m^2 k \cdot p}{4\pi\alpha q_0}, \quad (19)$$

$$\frac{d\sigma_C^{IPA}}{d\omega'} = \frac{\pi r_e^2 m^2}{\xi^2 k \cdot p} \sum_{n=1}^\infty \frac{\Theta(u_n - u)}{P_n} \left[ -4J_n^2 + \xi^2 \left( 2 + \frac{u^2}{1+u} \right) (J_{n-1}^2 + J_{n+1}^2 - 2J_n^2) \right] \quad (20)$$

with  $q_0 = \sqrt{E_e^2 - m^2} + \beta_p \omega$ ,  $\beta_p = \xi^2 \frac{m^2}{2q \cdot k}$ ,  $q \cdot k = k \cdot p$ , and arguments  $z = \frac{2n\xi}{\sqrt{1+\xi^2}} \frac{1}{u_n} \sqrt{u(u_n - u)}$  of the Bessel func-

<sup>4</sup> The value  $\chi = 1$  is special since the small- $u$  region of II and the large- $u$  region of I must be joint directly,  $II^< \otimes I^>$ , while for  $\chi < 1$  the small- $u$  region II and the small- $u$  region of I must be joint followed by the large- $u$  region of I,  $II^< \otimes I^< \otimes I^>$ . In the opposite case of  $\chi > 1$ , the small- $u$  region of II must be joint with the large- $u$  region of II followed by the large- $u$  region of I,  $II^< \otimes II^> \otimes I^>$ . This distinction becomes also evident when inspecting the differently shaped sections of the continuous curves  $dP/du$  as a function of  $u$  for several values of  $\chi$ .

<sup>5</sup> For recent work on the formalism, see [33–35, 77–79] which advance earlier investigations [80, 81].

<sup>6</sup> In laser pulses such an additional parameter is not needed [83].

<sup>7</sup> Strictly speaking, imposing a finite duration in the monochromatic laser beam model 2) turns it into a flat-top laser pulse model of class 1.1), exemplified in [59] and applied to the non-linear Compton process.

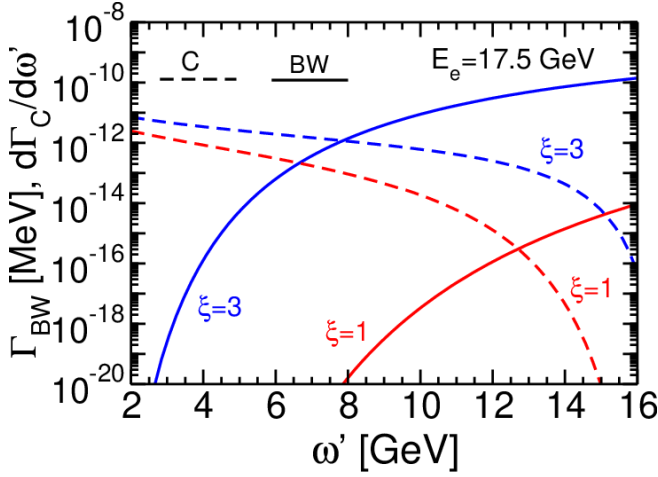


FIG. 5: The BW rate  $\Gamma_{BW}$  from Eqs. (17, 21) (solid curves) and the dimensionless differential C rate  $d\Gamma_C/d\omega'$  (dashed curves) from Eqs. (5, 16) as a function of  $\omega'$  for  $\xi = 1$  (red) and 3 (blue).

tions  $J_n$  as well as  $u_n = 2n \frac{\kappa_n p}{m^2} \frac{1}{1+\xi^2}$ ,  $u = \frac{n\omega - \omega'}{\kappa_n - n\omega + \omega'}$ ,  $\kappa_n = n\omega - \frac{1}{2}me^\zeta + \frac{1}{2}m(1+\xi^2)e^{-\zeta}$ ,  $P_n = m|n\frac{\omega}{m} - \sinh \zeta + \frac{\xi^2}{2}e^{-\zeta}|$ . These equations make the dependence  $u(\omega')$  explicit and relate again the differential cross section  $d\sigma/d\omega'$  with the differential rate  $d\Gamma/d\omega'$ . Since the BW rate is exceedingly small at small  $\omega'$  (see Fig. 5), improvements of the Compton rate by catching the details of harmonic structures there are less severe for the pair number Eq. (15).

Equation (18) of the BW rate, however, is inappropriate at smaller values of  $\xi$  [75] and needs improvement. Instead of using the series expansion in Bessel functions [58], a convenient formula is

$$\mathcal{F}_{BW} = \frac{1}{4\pi} \sum_{n=n_{min}}^{\infty} \int_1^{u_n} \frac{du}{u^{3/2}\sqrt{1-u}} \quad (21)$$

$$\times \exp\{-2n(a - \tanh a)\} \frac{1 + 2\xi^2(2u - 1) \sinh^2 a}{a \tanh a}$$

with  $n_{min} = 2\xi(1 + \xi^2)/\chi$  and  $u_n = n/n_{min}$ . This representation emerges from the large- $n$  approximation of Bessel functions,  $J_n(z) \approx \exp\{-n(a - \tanh a)\}/\sqrt{2n\pi \tanh a}$  and  $\tanh a = \sqrt{1 - z^2/n^2}$ . In the large- $\xi$  limit, one may replace the summation over  $n$  by an integration to arrive, via a double saddle point approximation, at the famous Ritus expression (18), which in turn is a complement of Eq. (6), see [58].

Numerical results are exhibited in Fig. 6 for  $E_e = 45$  GeV, 17.5 GeV and 8 GeV. One observes a stark rise of  $N^{e^+e^-}$  up to  $\xi \sim 4$ , which turns for larger values of  $\xi$  into a modest rise. To quantify that rise one can employ the ansatz  $N^{e^+e^-}(\xi, E_e) = N_0^{e^+e^-}(E_e) \xi^{p(\xi, E_e)}$ . Note that, by such a quantification of the  $\xi$  dependence, one gets rid of the normalization  $F_t$ . For  $E_e = 17.5$  GeV we find  $p(\xi \approx 1) \approx 20$  dropping to  $p(\xi \approx 20) \approx 2$ , see Fig. 7.

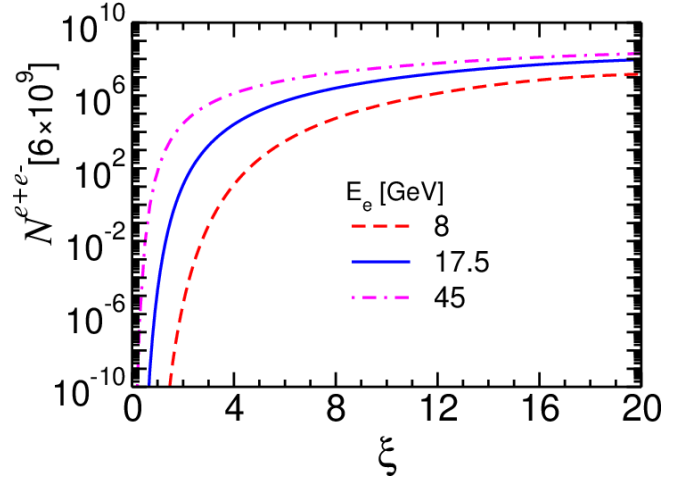


FIG. 6: The yield of  $e^+e^-$  pairs as a function of  $\xi$  for electron energies 45 GeV (magenta dash-dotted curve), 17.5 GeV (blue solid curve) and 8 GeV (red dashed curve) according to the probabilistic folding model  $C \otimes BW$  Eq. (15). For  $N_0^e = 6 \times 10^9$  electrons per bunch and per laser shot of duration  $NT_0$ . The special normalization  $F_t = T_0^2/2$  is chosen, as realized by  $T_{BW} = (T_0^2 + T_C^2)/(2T_C)$ . The choice  $T_C \approx T_0$  facilitates a Compton spectrum  $dN_C/d\omega' = T_C d\Gamma_C/d\omega'$  which agrees, for  $\xi = \mathcal{O}(1)$  and in the region  $\omega' < 10$  GeV, with a bremsstrahlung spectrum generated by electrons of the same energy impinging on a foil with  $X/X_0 = 0.01$  [75]. It is the  $\xi$  dependence of the Compton spectrum (see Fig. 5) which makes the pair yield more rapidly rising with  $\xi$  than the pair yield of the bremsstrahlung  $\otimes BW$  model in [75].

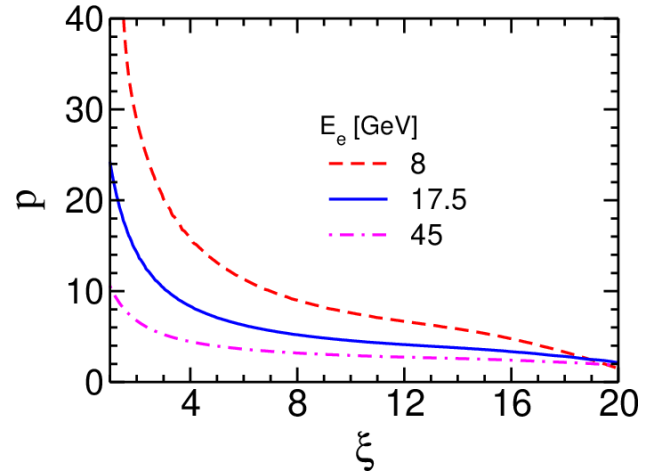


FIG. 7: The power  $p$  as a function of  $\xi$  for  $E_e = 45$  GeV (magenta dash-dotted curve), 17.5 GeV (blue solid curve) and 8 GeV (red dashed curve). The results exhibited in Fig. 6 are described by  $N^{e^+e^-}(\xi, E_e) = N_0^{e^+e^-}(E_e) \xi^{p(\xi, E_e)}$ .

Larger values of  $E_e$  reduce  $p$ , e.g.  $p(\xi \approx 1)|_{E_e=45 \text{ GeV}} \approx 10$  in agreement with [82], while  $p(\xi \approx 1)|_{E_e=8 \text{ GeV}} > 40$ . At  $\xi \rightarrow 20$ , a universal value of  $p \approx 2$  seems to emerge. The extreme nonlinear sensitivity of the pair number on the laser intensity parameter  $\xi$  at  $\xi < 10$ , and in particular at

$\xi \approx 1$ , points to the request of a refined and adequately realistic modeling beyond schematic approaches.

### C. Bandwidth effects in linear trident

The threshold for linear trident,  $e^- + \gamma(1.55 \text{ eV}) \rightarrow e^- + e^- + e^+$ , is at  $E_e = 337 \text{ GeV}$ , i.e. the LUXE kinematics is in the deep sub-threshold regime, where severe multi-photon effects build up the nonlinearity. However, also bandwidth effects can promote pair production in the sub-threshold region [84, 85], even at  $\xi \rightarrow 0$ . The key is the cross section of linear trident  $\sigma_{ppT}(\sqrt{\hat{s}}, \Delta\phi)$ , which depends on the invariant energy  $\sqrt{\hat{s}} = m\sqrt{1 + 2k \cdot p/m^2}$  and the pulse duration  $\Delta\phi$  for a given laser pulse. The quantity  $\sigma_{ppT}(\sqrt{\hat{s}}, \Delta\phi)$  is exhibited in Fig. 8 as a function of  $\sqrt{\hat{s}}$  for several values of  $\Delta\phi$ . For definiteness, we employ the laser pulse model of class 1.1) with parameterization  $\vec{A} = f_{ppT}(\phi) \vec{a}_x \cos \phi$  and envelope function  $f_{ppT} = \cos^2\left(\frac{\pi\phi}{2\Delta\phi}\right) \cap(\phi, 2\Delta\phi)$ , i.e. the number of laser-field oscillations within the pulse is  $N = \Delta\phi/\pi$ . In contrast to the presentation above, we deploy results in this sub-section for linear polarization and the  $\cos^2$  envelope.

We employ the formalism in [79] and its numerical implementation, that is “pulsed perturbative QED” in the spirit of Furry picture QED in a series expansion in powers of  $\xi$ . Applied to trident, the pulsed perturbative trident (ppT) arises from the diagrams

(double lines: Volkov wave functions, vertical lines: photon propagator) as leading-order term surviving  $\xi \rightarrow 0$ .

The scaled number of pairs is  $N_{tot}/N_0^e = 2\pi\Gamma_{tot}/\pi$ , where the probability rate is given by

$$\Gamma_{tot} = \sigma_{ppT} \frac{\omega}{2} \frac{m^2 \xi^2}{4\pi\alpha} \int_{-\infty}^{\infty} d\phi f_{ppT}^2(\phi). \quad (22)$$

The chosen pulse implies  $\int_{-\infty}^{\infty} d\phi f_{ppT}^2(\phi) = \frac{3}{2}\Delta\phi$  and  $N_{tot}/N_0^e = \sigma_{ppT} \frac{3m^2 \xi^2}{16\alpha} \Delta\phi$ . Note the  $\xi^2$  dependence from the “target density” already entering in Eq. (22) (cf. [84, 87] for analog relations). This is in contrast to Fig. 6, where genuine nonlinear effects are at work and mix with a stronger  $\xi$  dependence for  $C\otimes BW$ . The  $\xi^2$  dependence is characteristic for pair production by probe photons provided by an “external target”, such as in the bremsstrahlung-laser configuration of LUXE, cf. [75].

For the long laser pulses used in E-144 [88–90], such bandwidth effects are less severe.

## V. SUMMARY

In summary, inspired by the renewed interest in the Ritus-Narozhny conjecture and the new perspectives offered by the experimental capabilities of LUXE and E-320, we recollect a few features of elementary QED pro-

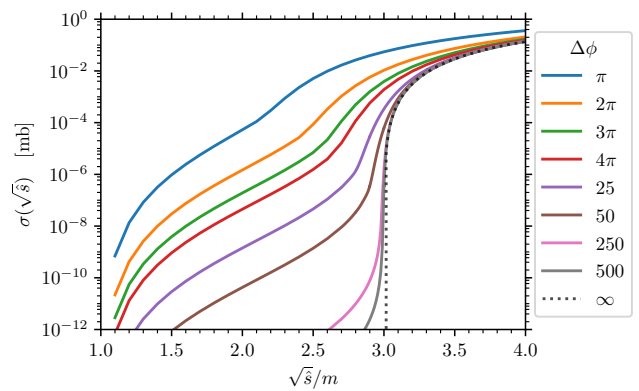


FIG. 8: Pulsed perturbative trident cross section  $\sigma_{ppT}$  as a function of  $\sqrt{\hat{s}}/m$  for several pulse lengths  $\Delta\phi$ . In the IPA limit, i.e. a monochromatic laser beam or  $\Delta\phi \rightarrow \infty$ , the threshold is at  $\sqrt{\hat{s}} = 3m$ . Above the threshold, the dots depict a few points (cf. table 1 in [86]) from perturbative trident without bandwidth effects. Bandwidth effects enable the pair production in the sub-threshold region  $\sqrt{\hat{s}} < 3m$ .

cesses within the essentially known formalism. In particular, we focus on the  $\xi$  dependence. For nonlinear Compton scattering, we point out that, in the non-asymptotic region  $\chi = \mathcal{O}(1)$ ,  $k \cdot p \lesssim m^2$ , the spectrally resolved cross section  $d\sigma/du|_{u=const}$  as a function of the laser intensity parameter  $\xi$  displays a pronounced  $\cap$  shape for  $u > u_{KN}$  (the “rise and fall”). This behavior is in stark contrast with the monotonously rising integrated probability  $\lim_{\chi, \xi \rightarrow \infty} \mathbb{P} \propto \alpha\chi^{2/3}m^2/k \cdot p$ . That is, in different regions of the phase space, also different sensitivities of cross sections/rates/probabilities on the laser intensity impact can be observed. The soft (small- $u$ ) part, which determines the integrated cross section/probability, may behave completely different than the hard (large- $u$ ) contribution.<sup>8</sup> Transferred to certain approximations used in simulation codes such a behavior implies that one should test differentially where the conditions for applicability are ensured.

The hard photons, once produced by Compton process in a laser pulse, act as seeds for secondary processes, most notably the Breit-Wheeler process. A folding model of type Compton $\otimes$ Breit-Wheeler on the probabilistic level points to a rapidly increasing rate of  $e^+e^-$  production in the region  $\xi \lesssim 4$ , when using parameters in reach of the planned LUXE set-up. The actual plans (see figure 2.10 in LUXE CDR [45]) uncover  $\xi = 2$  (40 TW, 8  $\mu\text{m}$

<sup>8</sup> An analog situation is known in QCD [91]: Tree-level diagrams are calculated primarily with constant  $\alpha_{QCD}$ . Renormalization improvement means then replacing  $\alpha_{QCD}$  by  $\alpha_{QCD}(\mathfrak{s})$  which accounts at the same time for all vertices in the considered diagram by one global scale  $\mathfrak{s}$ . Inserting explicitly loop corrections leads finally to scale dependent couplings  $\alpha_{QCD}(\mathfrak{s}_v)$  specific for each vertex  $v$  separately.

laser), 6 (40 TW, 3  $\mu\text{m}$ ) and 16 (300 TW, 3  $\mu\text{m}$ ), and E-320 envisages  $\xi = 10$ . The folding model may be utilized as reference to identify the occurrence of the wanted one-step trident process in this energy-intensity regime. Furthermore, bandwidth effects in the trident process are isolated by considering the weak-field regime  $\xi \rightarrow 0$ .

### Appendix A: Basics of nonlinear Compton process

Following [92] we recall the basics of the underlying formalism of the nonlinear Compton process. Within the Furry picture the lowest-order, tree-level  $S$  matrix element for the one-photon (four-momentum  $k'$ , four-polarization  $\epsilon'$ ) decay of a laser-dressed electron  $e_L$  in the background field (1)  $e_L(p) \rightarrow e_L(p') + \gamma(k', \epsilon')$  reads with suitable normalizations of the wave functions

$$S_{fi} = -ie \int d^4x J \cdot \epsilon'^* \exp\{ik' \cdot x\} \quad (\text{A1})$$

where the current  $J_\mu(x) = \bar{\Psi}_{p'} \gamma_\mu \Psi_p$  is built by the Volkov wave function  $\Psi_p = E_p u_p \exp\{-ip \cdot x\} \exp\{-if_p\}$  (spin indices are suppressed) and its adjoint  $\bar{\Psi}$  with Ritus matrix  $E_p = 1 + \frac{e}{2k \cdot p} \not{k} \not{A}$  and phase function  $f_p(\phi) = \frac{e}{k \cdot p} \int_0^\phi d\phi' [p \cdot A - \frac{e}{2} A \cdot A]$ . We employ Feynman's slash notation and denote scalar products by the dot between four-vectors;  $u_p$  is the free Dirac bi-spinor. Exploiting the symmetry of the background field,  $A(\phi = k \cdot x)$ , Eq. (A1) can be manipulated (cf. [92] for details) to arrive at

$$S_{fi} = -ie(2\pi)^3 \frac{2}{k_-} \delta^{(3)}(\underline{p} - \underline{p}' - \underline{k}') \mathcal{M}(\ell), \quad (\text{A2})$$

where  $\ell \equiv (k'_- + p'_- - p_-)/k_- = k' \cdot p/k \cdot p'$  accomplishes the balance equation  $p + \ell k - p' - k' = 0$ . (See [62] for a formulation with  $S_{fi} = -ie(2\pi)^4 \int \frac{d\ell}{2\pi} \delta^{(4)}(p + \ell k - p' - k') \mathcal{M}(\ell)$ .) Light-cone coordinates are useful here, e.g.  $k_- = k^0 - k^3$ ,  $k_+ = k^0 + k^3$ ,  $k_\perp = (k^1, k^2)$ , and  $\underline{k} = (k_+, k_\perp)$ . Imposing gauge invariance yields the matrix element

$$\mathcal{M} = \sum_{i=1}^3 J^{(i)} S^{(i)} \quad (\text{A3})$$

with the pieces of the electron current

$$\hat{j}^{(0)} = \bar{u}_{p'} \not{\epsilon}'^* u_p, \quad (\text{A4})$$

$$\hat{j}^{(1,2)} = \bar{u}_{p'} \left( d_{p'} \not{\epsilon}'_\pm \not{k} \not{\epsilon}'^* + d_p \not{\epsilon}'^* \not{k} \not{\epsilon}'_\pm \right) u_p, \quad (\text{A5})$$

$$\hat{j}^{(3)} = 4k \cdot \epsilon'^* d_{p'} d_p \bar{u}_{p'} \not{k} u_p, \quad (\text{A6})$$

which combine to  $J^{(1,2)} = \hat{j}^{(1,2)} + \frac{\alpha_\pm}{2\ell} \hat{j}^{(0)}$ ,  $J^{(3)} = \hat{j}^{(3)} + \frac{\beta}{\ell} \hat{j}^{(0)}$ . The following abbreviations are used:  $d_p = \frac{m\xi}{4k \cdot p}$  and  $d_{p'} = \frac{m\xi}{4k \cdot p'}$ ,  $\alpha_\pm = m\xi \left( \frac{\epsilon_\pm \cdot p}{k \cdot p} - \frac{\epsilon_\pm \cdot p'}{k \cdot p'} \right)$  with  $\vec{\epsilon}_\pm = (\vec{a}_x \pm i\vec{a}_y) e^2/m^2 \xi^2$  and  $\beta = \frac{m^2 \xi^2}{4} \left( \frac{1}{k \cdot p} - \frac{1}{k \cdot p'} \right)$  as well.

The phase integrals  $S^{(i)}$  are the remainders of the integration  $d^4x = d\phi dx_- d^2x_\perp/k_-$  in Eq. (A1):

$$\begin{aligned} S^{(1,2)} &= \int_{-\infty}^{\infty} d\phi f(\phi) \exp\{i(\ell \pm 1)\phi - i(f_p(\phi) - f_{p'}(\phi))\}, \\ S^{(3)} &= \int_{-\infty}^{\infty} d\phi f^2(\phi) \exp\{i\ell\phi - i(f_p(\phi) - f_{p'}(\phi))\} \\ &\quad \times [1 + \cos 2\phi]. \end{aligned} \quad (\text{A7})$$

For a few special non-unipolar (plane-wave) fields and their envelopes  $f(\phi)$ , the phase integrals can be processed exactly by analytic means [93, 94], but in general a numerical evaluation is needed. The very special IPA case of  $f(\phi) = 1$  allows for a simple representation of  $f_p(\phi)$  with subsequent decomposition of  $S^{(i)}$  into Bessel functions, yielding final expressions as in Eqs. (2, 20).

For identifying the weak-field limit,  $\xi \rightarrow 0$ , it is necessary to recognize in Eq. (A3)  $J^{(0)} \propto \xi^0$ , and  $\alpha_\pm, J^{(1,2)} \propto \xi^1$ , and  $\beta, J^{(3)} \propto \xi^2$ . Thus,  $\lim_{\xi \rightarrow 0} \mathcal{M} = \mathcal{M}_1 \xi + \mathcal{M}_2 \xi^2 + \dots$ . We emphasize the Fourier transform of the pulse envelope,  $\lim_{\xi \rightarrow 0} S^{(1,2)} = \int_{-\infty}^{\infty} d\phi f(\phi) \exp\{i(\ell \pm 1)\phi\}$ , entering  $\mathcal{M}_1$ , where only  $S^{(1)}$  with  $\ell \geq 0$  contributes to the wanted one-photon emission:<sup>9</sup>  $\mathcal{M}_1(\ell) = J^{(1)} \int_{-\infty}^{\infty} d\phi f(\phi) \exp\{i(\ell - 1)\phi\}$ ,  $J^{(1)}(\ell) = \frac{m}{2} \epsilon'_\mu \epsilon_{+\nu} \bar{u}_{p'} \left[ \frac{\gamma^\mu \not{k}_\perp \gamma^\nu + 2\gamma^\mu p^\nu}{2k_\perp \cdot p} + \frac{\gamma^\nu \not{k}'_\perp \gamma^\mu - 2\gamma^\nu p^\mu}{2k'_\perp \cdot p} \right] u_p$  with  $k_\ell \equiv \ell k$ . For pulses with broad support,  $f(\phi) \rightarrow 1$ , within the interval  $\Delta\phi \gg 1$ , one arrives at the standard Compton (Klein-Nishina) expression in leading order by using  $\xi \rightarrow 2e/m$ . The appearance of  $\delta(\ell - 1)$  combined with the definition of  $\ell$  below Eq. (A2) leads to the famous Compton formula via  $\delta\left(\omega' - \frac{\omega m}{m + \omega(1 - \cos\Theta')}\right)$  in the electron's rest frame by the subsequent phase space integration(s).

The discussion of the large- $\xi$  limit needs some care in general, cf. [26, 28]. Useful limits are obtained for the IPA case [58] under the side condition  $\xi^2(1 - z^2/n^2) = \text{const}$  (cf. Eqs. (19, 20)), e.g.  $|\mathcal{M}|^2|_{u \ll 1} \propto (\xi/u)^{2/3}$  and  $|\mathcal{M}|^2|_{u \gg 1} \propto u^{-1}(\xi/u)^{1/2} \exp\{-\frac{2u}{3\xi} \frac{m^2}{k \cdot p}\} \rightarrow \sqrt{\xi}$  (cf. Eqs. (14) and (13)). At  $\xi \gg 1$ , the  $\xi$  and  $u$  dependencies of resulting probabilities for circular polarization and constant cross field backgrounds coincide.

These limits are at the heart of the ‘‘rise and fall’’.

The differential emission probability per *in*-electron and per laser pulse follows from (A2) by partial integration over the *out*-phase space,

$$\frac{d\mathbb{P}}{d\omega' d\Omega'} = \frac{e^2 \omega'}{64\pi^3 k \cdot p k \cdot p'} |\mathcal{M}|^2, \quad (\text{A8})$$

and may be transformed to other coordinates, e.g.  $u$  or  $\ell$  etc. Having in mind the IPA limit, one should turn to

<sup>9</sup> The same reasoning applies in IV C for one-pair emission, i.e. the finite-width Fourier transform of  $f(\phi)$  at  $\Delta\phi < \infty$  enables the sub-threshold pair production  $e_L(p) \rightarrow e_L(p') + e_L(p'') + \bar{e}_L(p''')$ .

the dimensionless differential rate [62]

$$\frac{d\Gamma_C}{d\omega' d\Omega'} = \frac{e^2 \omega'}{32\pi^2 q_0 k \cdot p'} |\mathcal{M}|^2. \quad (\text{A9})$$

Spin averaging of the *in*-electron, and spin summation of the *out*-electron and summation over the *out*-photon polarizations leads to  $|\overline{\mathcal{M}}|^2$ , unless one is interested in polarization effects as in [19, 20, 95]. The above expressions (A3 - A7) can be further processed for special field envelopes, or  $|\mathcal{M}|^2$  is numerically accessible, via Eq. (A3), as mod-squared sum of complex number products provided by Eqs. (A4 - A7) which need afterwards explicit (numerical) spin and polarization summation/averaging to arrive at  $|\overline{\mathcal{M}}|^2$ .

The cross section is obtained by normalization on

the integrated laser photon flux:  $d\sigma = d\Gamma_C \frac{q_0 \cdot \omega}{k \cdot p n_L}$  with  $n_L = \frac{m^2}{e^2} \xi^2 \omega N_L$ , where  $N_L = 1$  (IPA, quasi-momentum  $q_0$ ) or  $N_L = \frac{1}{2\pi} \int_{-\infty}^{\infty} d\phi f(\phi)$  (FPA,  $q_0 \equiv p_0$ ). The circularly polarized laser background (1) is supposed in these relations.

### Acknowledgments

The authors gratefully acknowledge the collaboration with D. Seipt, T. Nusch, T. Heinzl, and useful discussions with A. Ilderton, K. Krajewska, M. Marklund, C. Müller, S. Rykovanov, and G. Torgrimsson. A. Ringwald and B. King are thanked for explanations w.r.t. LUXE. The work is supported by R. Sauerbrey and T. E. Cowan w.r.t. the study of fundamental QED processes for HIBEF.

- 
- [1] M. E. Peskin and D. V. Schroeder, “An Introduction to Quantum Field Theory,” Addison-Wesley, Reading (1995).
- [2] G. Abbiendi *et al.* [OPAL Collaboration], “Measurement of the running of the QED coupling in small-angle Bhabha scattering at LEP,” *Eur. Phys. J. C* **45**, 1 (2006) [hep-ex/0505072].
- [3] I. Arapoglou *et al.*, “g Factor of Boronlike Argon Ar40<sup>13+</sup>,” *Phys. Rev. Lett.* **122**, no. 25, 253001 (2019) [arXiv:1906.00881 [physics.atom-ph]].
- [4] S. Alighanbari, G. S. Giri, F. L. Constantin, *et al.*, “Precise test of quantum electrodynamics and determination of fundamental constants with HD+ ions,” *Nature* **581**, 152–158 (2020).
- [5] T. Aoyama *et al.*, “The anomalous magnetic moment of the muon in the Standard Model,” *Phys. Rept.* **887**, 1 (2020) [arXiv:2006.04822 [hep-ph]].
- [6] V. Ritus, “Radiative Effects and Their Enhancement in an Intense Electromagnetic Field,” *Sov. Phys. JETP* **30**, 1181 (1970).
- [7] D. Morozov and N. Narozhny, “Elastic scattering of photons in an intense field and the photoproduction of a pair and a photon,” *Sov. Phys. JETP* **45**, 23 (1977).
- [8] N. Narozhny, “Radiation corrections to quantum processes in an intense electromagnetic field,” *Phys. Rev. D* **20**, 1313 (1979).
- [9] N. Narozhny, “Expansion parameter of perturbation theory in intense-field quantum electrodynamics,” *Phys. Rev. D* **21**, 1176 (1980).
- [10] D. Morozov, N. Narozhny and V. I. Ritus, “Vertex function of an electron in a constant electromagnetic field,” *Sov. Phys. JETP* **53**, 1103 (1981).
- [11] A. A. Mironov, S. Meuren and A. M. Fedotov, “Resummation of QED radiative corrections in a strong constant crossed field,” *Phys. Rev. D* **102**, no. 5, 053005 (2020) [arXiv:2003.06909 [hep-th]].
- [12] T. Heinzl, A. Ilderton and B. King, “Classical resummation and breakdown of strong-field QED,” arXiv:2101.12111 [hep-ph].
- [13] J. P. Edwards and A. Ilderton, “Resummation of background-collinear corrections in strong field QED,” *Phys. Rev. D* **103**, no. 1, 016004 (2021) [arXiv:2010.02085 [hep-ph]].
- [14] A. M. Fedotov, “Conjecture of perturbative QED breakdown at  $\alpha\chi^{2/3} \gtrsim 1$ ,” *J. Phys. Conf. Ser.* **826**, no. 1, 012027 (2017) [arXiv:1608.02261 [hep-ph]].
- [15] N. Brambilla *et al.*, “QCD and Strongly Coupled Gauge Theories: Challenges and Perspectives,” *Eur. Phys. J. C* **74**, no. 10, 2981 (2014) [arXiv:1404.3723 [hep-ph]].
- [16] R. V. Popov *et al.*, “How to access QED at a supercritical Coulomb field,” *Phys. Rev. D* **102**, no. 7, 076005 (2020) [arXiv:2008.05005 [hep-ph]].
- [17] V. Yakimenko *et al.*, “Prospect of Studying Nonperturbative QED with Beam-Beam Collisions,” *Phys. Rev. Lett.* **122**, no. 19, 190404 (2019) [arXiv:1807.09271 [physics.plasm-ph]].
- [18] A. Di Piazza, “Unveiling the transverse formation length of nonlinear Compton scattering,” *Phys. Rev. A* **103**, no. 1, 012215 (2021) [arXiv:2009.00526 [hep-ph]].
- [19] D. Seipt and B. King, “Spin- and polarization-dependent locally-constant-field-approximation rates for nonlinear Compton and Breit-Wheeler processes,” *Phys. Rev. A* **102**, no. 5, 052805 (2020) [arXiv:2007.11837 [physics.plasm-ph]].
- [20] B. King and S. Tang, “Nonlinear Compton scattering of polarized photons in plane-wave backgrounds,” *Phys. Rev. A* **102**, no. 2, 022809 (2020) [arXiv:2003.01749 [hep-ph]].
- [21] A. I. Titov, B. Kämpfer and H. Takabe, “Nonlinear Breit-Wheeler process in short laser double pulses,” *Phys. Rev. D* **98**, no. 3, 036022 (2018) [arXiv:1807.04547 [physics.plasm-ph]].
- [22] A. Ilderton, B. King and S. Tang, “Toward the observation of interference effects in nonlinear Compton scattering,” *Phys. Lett. B* **804**, 135410 (2020) [arXiv:2002.04629 [physics.atom-ph]].
- [23] L. F. Granz, O. Mathiak, S. Villalba-Chávez and C. Müller, “Electron-positron pair production in oscillating electric fields with double-pulse structure,” *Phys. Lett. B* **793**, 85 (2019) [arXiv:1903.06000 [physics.plasm-ph]].
- [24] T. G. Blackburn, A. J. MacLeod and B. King, “From local to nonlocal: higher fidelity simulations of photon emission in intense laser pulses,” arXiv:2103.06673 [hep-ph].

- ph].
- [25] T. Heinzl, B. King and A. J. Macleod, “The locally monochromatic approximation to QED in intense laser fields,” *Phys. Rev. A* **102**, 063110 (2020) [arXiv:2004.13035 [hep-ph]].
- [26] A. Ilderton, B. King and D. Seipt, “Extended locally constant field approximation for nonlinear Compton scattering,” *Phys. Rev. A* **99**, no. 4, 042121 (2019) [arXiv:1808.10339 [hep-ph]].
- [27] T. G. Blackburn, D. Seipt, S. S. Bulanov and M. Marklund, “Benchmarking semiclassical approaches to strong-field QED: nonlinear Compton scattering in intense laser pulses,” *Phys. Plasmas* **25**, no. 8, 083108 (2018) [arXiv:1804.11085 [physics.plasm-ph]].
- [28] A. Di Piazza, M. Tamburini, S. Meuren and C. H. Keitel, “Improved local-constant-field approximation for strong-field QED codes,” *Phys. Rev. A* **99**, no. 2, 022125 (2019) [arXiv:1811.05834 [hep-ph]].
- [29] V. N. Khudik *et al.*, “Towards realistic simulations of QED cascades: Non-ideal laser and electron seeding effects,” *Phys. Plasmas* **25**, no. 8, 083104 (2018) [arXiv:1807.09747 [physics.plasm-ph]].
- [30] T. G. Blackburn, A. Ilderton, C. D. Murphy and M. Marklund, “Scaling laws for positron production in laser–electron-beam collisions,” *Phys. Rev. A* **96**, no. 2, 022128 (2017) [arXiv:1708.00298 [physics.plasm-ph]].
- [31] A. Gonoskov *et al.*, “Extended particle-in-cell schemes for physics in ultrastrong laser fields: Review and developments,” *Phys. Rev. E* **92**, no. 2, 023305 (2015) [arXiv:1412.6426 [physics.plasm-ph]].
- [32] G. Torgrimsson, “Loops and polarization in strong-field QED,” arXiv:2012.12701 [hep-ph].
- [33] G. Torgrimsson, “Nonlinear trident in the high-energy limit: Nonlocality, Coulomb field and resummations,” *Phys. Rev. D* **102**, no. 9, 096008 (2020) [arXiv:2007.08492 [hep-ph]].
- [34] V. Dinu and G. Torgrimsson, “Trident process in laser pulses,” *Phys. Rev. D* **101**, no. 5, 056017 (2020) [arXiv:1912.11017 [hep-ph]].
- [35] V. Dinu and G. Torgrimsson, “Approximating higher-order nonlinear QED processes with first-order building blocks,” *Phys. Rev. D* **102**, no. 1, 016018 (2020) [arXiv:1912.11015 [hep-ph]].
- [36] A. Di Piazza, C. Müller, K. Z. Hatsagortsyan and C. H. Keitel, “Extremely high-intensity laser interactions with fundamental quantum systems,” *Rev. Mod. Phys.* **84**, 1177 (2012) [arXiv:1111.3886 [hep-ph]].
- [37] A. Ilderton, “Note on the conjectured breakdown of QED perturbation theory in strong fields,” *Phys. Rev. D* **99**, no. 8, 085002 (2019) [arXiv:1901.00317 [hep-ph]].
- [38] T. Podszus and A. Di Piazza, “High-energy behavior of strong-field QED in an intense plane wave,” *Phys. Rev. D* **99**, no. 7, 076004 (2019) [arXiv:1812.08673 [hep-ph]].
- [39] S. Meuren, “Probing Strong-field QED at FACET-II (SLAC E-320) (2019)”, [https://conf.slac.stanford.edu/facet-2-2019/sites/facet-2-2019.conf.slac.stanford.edu/files/basic-page-docs/sfqed\\_2019.pdf](https://conf.slac.stanford.edu/facet-2-2019/sites/facet-2-2019.conf.slac.stanford.edu/files/basic-page-docs/sfqed_2019.pdf).
- [40] S. Meuren *et al.*, “On Seminal HEDP Research Opportunities Enabled by Colocating Multi-Petawatt Laser with High-Density Electron Beams,” arXiv:2002.10051 [physics.plasm-ph].
- [41] K. Poder *et al.*, “Experimental Signatures of the Quantum Nature of Radiation Reaction in the Field of an Ultra-intense Laser,” *Phys. Rev. X* **8**, no. 3, 031004 (2018) [arXiv:1709.01861 [physics.plasm-ph]].
- [42] J. M. Cole *et al.*, “Experimental evidence of radiation reaction in the collision of a high-intensity laser pulse with a laser-wakefield accelerated electron beam,” *Phys. Rev. X* **8**, no. 1, 011020 (2018) [arXiv:1707.06821 [physics.plasm-ph]].
- [43] C. Keitel *et al.*, “Photo-induced pair production and strong field QED on Gemini,” arXiv:2103.06059 [physics.plasm-ph].
- [44] H. Abramowicz *et al.*, “Letter of Intent for the LUXE Experiment,” arXiv:1909.00860 [physics.ins-det].
- [45] H. Abramowicz *et al.*, “Conceptual Design Report for the LUXE Experiment,” arXiv:2102.02032 [hep-ex].
- [46] U. Hernandez Acosta, A. Otto, B. Kämpfer and A. I. Titov, “Non-perturbative signatures of non-linear Compton scattering,” *Phys. Rev. D* **102**, 024914 (2020) [arXiv:2001.03986 [hep-ph]].
- [47] B. Kämpfer and A. I. Titov, “Impact of laser polarization on q-exponential photon tails in non-linear Compton scattering,” *Phys. Rev. A* **103**, 033101 (2021) [arXiv:2012.07699 [hep-ph]].
- [48] A. Jochmann *et al.*, “High Resolution Energy-Angle Correlation Measurement of Hard X Rays from Laser-Thomson Backscattering,” *Phys. Rev. Lett.* **111**, no. 11, 114803 (2013).
- [49] I. C. E. Turcu *et al.*, “High field physics and QED experiments at ELI-NP,” *Rom. Rep. Phys.* **68**, no. Supplement, S145 (2016).
- [50] HIBEF: Helmholtz International Beam Line for Extreme Fields, cf. <https://www.hzdr.de/db/Cms?pOid=50566&pNid=694>
- [51] A. Di Piazza, “WKB electron wave functions in a tightly focused laser beam,” *Phys. Rev. D* **103**, no. 7, 076011 (2021) [arXiv:2102.06692 [hep-ph]].
- [52] A. Di Piazza, “First-order strong-field QED processes in a tightly focused laser beam,” *Phys. Rev. A* **95**, no. 3, 032121 (2017) [arXiv:1612.04132 [hep-ph]].
- [53] T. Heinzl and A. Ilderton, “Exact classical and quantum dynamics in background electromagnetic fields,” *Phys. Rev. Lett.* **118**, no. 11, 113202 (2017) [arXiv:1701.09166 [hep-ph]].
- [54] F. Karbstein and E. A. Mosman, “Enhancing quantum vacuum signatures with tailored laser beams,” *Phys. Rev. D* **101**, no. 11, 113002 (2020) [arXiv:2004.04268 [quant-ph]].
- [55] A. Blinne, H. Gies, F. Karbstein, C. Kohlfürst and M. Zepf, “All-optical signatures of quantum vacuum nonlinearities in generic laser fields,” *Phys. Rev. D* **99**, no. 1, 016006 (2019) [arXiv:1811.08895 [physics.optics]].
- [56] F. Karbstein and E. A. Mosman, “Photon polarization tensor in pulsed Hermite- and Laguerre-Gaussian beams,” *Phys. Rev. D* **96**, no. 11, 116004 (2017) [arXiv:1711.06151 [hep-ph]].
- [57] V. Dinu, T. Heinzl and A. Ilderton, “Infra-Red Divergences in Plane Wave Backgrounds,” *Phys. Rev. D* **86**, 085037 (2012) [arXiv:1206.3957 [hep-ph]].
- [58] V. I. Ritus, “Quantum effects of the interaction of elementary particles with an intense electromagnetic field,” *J. Sov. Laser Res. (United States)* **6**, 497 (1985).
- [59] B. King, “Pulse envelope effect on nonlinear Compton scattering in electron-laser collisions,” *Phys. Rev. D* **103**, no. 3, 036018 (2021) [arXiv:2012.05920 [hep-ph]].
- [60] A. Otto, D. Seipt, D. Blaschke, B. Kämpfer and

- S. A. Smolyansky, “Lifting shell structures in the dynamically assisted Schwinger effect in periodic fields,” *Phys. Lett. B* **740**, 335 (2015) [arXiv:1412.0890 [hep-ph]].
- [61] A. Otto, H. Oppitz and B. Kämpfer, “Assisted Vacuum Decay by Time Dependent Electric Fields,” *Eur. Phys. J. A* **54**, no. 2, 23 (2018) [arXiv:1801.09943 [hep-ph]].
- [62] A. I. Titov, B. Kämpfer, A. Hosaka and H. Takabe, “Quantum processes in short and intensive electromagnetic fields,” *Phys. Part. Nucl.* **47**, no. 3, 456 (2016) [arXiv:1512.07987 [hep-ph]].
- [63] A. I. Titov, B. Kämpfer, T. Shibata, A. Hosaka and H. Takabe, “Laser pulse-shape dependence of Compton scattering,” *Eur. Phys. J. D* **68**, no. 10, 299 (2014) [arXiv:1408.1040 [hep-ph]].
- [64] A. I. Titov, A. Otto and B. Kämpfer, “Multi-photon regime of non-linear Breit-Wheeler and Compton processes in short linearly and circularly polarized laser pulses,” *Eur. Phys. J. D* **74**, no. 2, 39 (2020) [arXiv:1907.00643 [physics.plasm-ph]].
- [65] A. I. Titov, B. Kämpfer, H. Takabe and A. Hosaka, “Neutrino pair emission off electrons in a strong electromagnetic wave field,” *Phys. Rev. D* **83**, 053008 (2011) [arXiv:1011.4860 [hep-ph]].
- [66] K. Fleck, N. Cavanagh and G. Sarri, “Conceptual Design of a High-flux Multi-GeV Gamma-ray Spectrometer,” *Sci. Rep.* **10**, no. 1, 9894 (2020).
- [67] J. Z. Kamiński, K. Krajewska and F. Ehlötzky, “Monte Carlo analysis of electron-positron pair creation by powerful laser-ion impact,” *Phys. Rev. A* **74**, no. 3, 033402 (2006).
- [68] T. Heinzl, A. Ilderton and M. Marklund, “Finite size effects in stimulated laser pair production,” *Phys. Lett. B* **692**, 250 (2010) [arXiv:1002.4018 [hep-ph]].
- [69] K. Krajewska and J. Z. Kamiński, “Breit-Wheeler Process in Intense Short Laser Pulses,” *Phys. Rev. A* **86**, 052104 (2012) [arXiv:1209.2394 [hep-ph]].
- [70] K. Krajewska and J. Z. Kamiński, “Coherent combs of antimatter from nonlinear electron-positron-pair creation,” *Phys. Rev. A* **90**, no. 5, 052108 (2014) [arXiv:1407.4101 [hep-ph]].
- [71] M. J. A. Jansen, J. Z. Kamiński, K. Krajewska and C. Müller, “Strong-field Breit-Wheeler pair production in short laser pulses: Relevance of spin effects,” *Phys. Rev. D* **94**, 013010 (2016) [arXiv:1605.03476 [hep-ph]].
- [72] M. J. A. Jansen and C. Müller, “Strong-Field Breit-Wheeler Pair Production in Two Consecutive Laser Pulses with Variable Time Delay,” *Phys. Lett. B* **766**, 71 (2017) [arXiv:1612.07137 [quant-ph]].
- [73] A. I. Titov and B. Kämpfer, “Non-linear Breit-Wheeler process with linearly polarized beams,” *Eur. Phys. J. D* **74**, no. 11, 218 (2020) [arXiv:2006.04496 [hep-ph]].
- [74] A. Golub, S. Villalba-Chávez, H. Ruhl and C. Müller, “Linear Breit-Wheeler pair production by high-energy bremsstrahlung photons colliding with an intense X-ray laser pulse,” *Phys. Rev. D* **103**, no. 1, 016009 (2021) [arXiv:2010.03871 [hep-ph]].
- [75] A. Hartin, A. Ringwald and N. Tapia, “Measuring the Boiling Point of the Vacuum of Quantum Electrodynamics,” *Phys. Rev. D* **99**, no. 3, 036008 (2019) [arXiv:1807.10670 [hep-ph]].
- [76] A. I. Titov, B. Kämpfer and H. Takabe, “Dimuon production by laser-wakefield accelerated electrons,” *Phys. Rev. ST Accel. Beams* **12**, 111301 (2009) [arXiv:0907.3038 [physics.acc-ph]].
- [77] B. King and A. M. Fedotov, “Effect of interference on the trident process in a constant crossed field,” *Phys. Rev. D* **98**, no. 1, 016005 (2018) [arXiv:1801.07300 [hep-ph]].
- [78] F. Mackenroth and A. Di Piazza, “Nonlinear trident pair production in an arbitrary plane wave: a focus on the properties of the transition amplitude,” *Phys. Rev. D* **98**, no. 11, 116002 (2018) [arXiv:1805.01731 [hep-ph]].
- [79] U. Hernandez Acosta and B. Kämpfer, “Laser pulse-length effects in trident pair production,” *Plasma Phys. Control. Fusion* **61**, no. 8, 084011 (2019) [arXiv:1901.08860 [hep-ph]].
- [80] V. N. Baier, V. M. Katkov and V. M. Strakhovenko, “Higher-order effects in external field - pair production by a particle,” *Yad. Fiz.* **14**, 1020 (1971).
- [81] V. I. Ritus, “Vacuum polarization correction to elastic electron and muon scattering in an intense field and pair electro- and muoproduction,” *Nucl. Phys. B* **44**, 236 (1972).
- [82] H. Hu, C. Muller and C. H. Keitel, “Complete QED theory of multiphoton trident pair production in strong laser fields,” *Phys. Rev. Lett.* **105**, 080401 (2010) [arXiv:1002.2596 [physics.atom-ph]].
- [83] A. Ilderton, “Trident pair production in strong laser pulses,” *Phys. Rev. Lett.* **106**, 020404 (2011) [arXiv:1011.4072 [hep-ph]].
- [84] A. I. Titov, H. Takabe, B. Kämpfer and A. Hosaka, “Enhanced subthreshold electron-positron production in short laser pulses,” *Phys. Rev. Lett.* **108**, 240406 (2012) [arXiv:1205.3880 [hep-ph]].
- [85] T. Nusch, D. Seipt, B. Kämpfer and A. I. Titov, “Pair production in short laser pulses near threshold,” *Phys. Lett. B* **715**, 246 (2012).
- [86] E. Haug, “Bremsstrahlung and Pair Production in the Field of Free Electrons,” *Z. Naturforsch. A* **30**, 1099 (1975).
- [87] D. Seipt and B. Kämpfer, “Non-Linear Compton Scattering of Ultrashort and Ultraintense Laser Pulses,” *Phys. Rev. A* **83**, 022101 (2011) [arXiv:1010.3301 [hep-ph]].
- [88] C. Bamber *et al.*, “Studies of nonlinear QED in collisions of 46.6-GeV electrons with intense laser pulses,” *Phys. Rev. D* **60**, 092004 (1999).
- [89] D. L. Burke *et al.*, “Positron production in multi-photon light by light scattering,” *Phys. Rev. Lett.* **79**, 1626 (1997).
- [90] C. Bula *et al.* [E144 Collaboration], “Observation of nonlinear effects in Compton scattering,” *Phys. Rev. Lett.* **76**, 3116 (1996).
- [91] W. A. Horowitz and Y. V. Kovchegov, “Running Coupling Corrections to High Energy Inclusive Gluon Production,” *Nucl. Phys. A* **849**, 72 (2011) [arXiv:1009.0545 [hep-ph]].
- [92] D. Seipt, “Strong-Field QED Processes in Short Laser Pulses,” PhD thesis, TU Dresden (2012).
- [93] D. Seipt, V. Kharin, S. Rykovanov, A. Surzhykov and S. Fritzsche, “Analytical results for nonlinear Compton scattering in short intense laser pulses,” *J. Plasma Phys.* **82**, no. 2, 655820203 (2016) [arXiv:1601.00442 [hep-ph]].
- [94] V. Dinu, “Exact final state integrals for strong field QED,” *Phys. Rev. A* **87**, no. 5, 052101 (2013) [arXiv:1302.1513 [hep-ph]].
- [95] D. Y. Ivanov, G. L. Kotkin and V. G. Serbo, “Complete description of polarization effects in e+e- pair production by a photon in the field of a strong laser wave,” *Eur. Phys. J. C* **40**, 27 (2005) [hep-ph/0412032].